Experimental and computational characterization of carbon fibre based structural battery electrode laminae

Downloaded from: https://research.chalmers.se, 2026-04-02 22:59 UTC

Citation for the original published paper (version of record):
Carlstedt, D., Rittweger, F., Runesson, K. et al (2022). Experimental and computational characterization of carbon fibre based structural battery electrode laminae. Composites Science and Technology, 220.
http://dx.doi.org/10.1016/j.compscitech.2022.109283

N.B. When citing this work, cite the original published paper.

research.chalmers.se offers the possibility of retrieving research publications produced at Chalmers University of Technology. It covers all kind of research output: articles, dissertations, conference papers, reports etc. since 2004. research.chalmers.se is administrated and maintained by Chalmers Library

(article starts on next page)

Composites Science and Technology 220 (2022) 109283

Contents lists available at ScienceDirect

Composites Science and Technology

journal homepage: www.elsevier.com/locate/compscitech

Experimental and computational characterization of carbon fibre based structural battery electrode laminae

David Carlstedt [a,*], Florian Rittweger [b], Kenneth Runesson [a], Adriana M. Navarro-Suárez [c,1], Johanna Xu [a], Shanghong Duan [a], Fredrik Larsson [a], Karl-Ragmar Riemschneider [b], Leif E. Asp [a]

[a] Chalmers University of Technology, Department of Industrial and Materials Science, 412 96, Gothenburg, Sweden
[b] Hamburg University of Applied Sciences, Department of Information and Electrical Engineering, 20099, Hamburg, Germany
[c] Chalmers University of Technology, Department of Physics, 412 96, Gothenburg, Sweden

ARTICLE INFO

Keywords:
Carbon fibres
Multifunctional composites
Electro-chemical behaviour
Electro-mechanical behaviour
Biomimetics

ABSTRACT

In this paper, electrode laminae consisting of carbon fibres embedded in structural battery electrolyte (CF-SBE electrodes) are characterized with respect to their multifunctional (i.e. combined electrochemical and mechanical) performance utilizing experimental and numerical techniques. The studied material is made from commercially available polyacrylonitrile (PAN)-based carbon fibres and a porous SBE matrix/electrolyte, which is composed of two continuous phases: a solid polymer skeleton (vinyl ester-based) and a Li-salt containing liquid electrolyte. Experimental and numerical studies are performed on CF-SBE electrode half-cells, whereby a coupled electro-chemo-mechanical finite element model is exploited. Results show that, similar to traditional batteries, electrode thickness, transport properties of the electrolyte and applied current significantly affect electrochemical performance. For example, increasing the electrode thickness of the studied CF-SBE electrode from 50 μm to 200 μm results in a reduction in specific capacity of approximately 70/95% for an applied current of 30/120 mA g^{-1} of fibres, respectively. Further, Li-insertion induced longitudinal expansion of carbon fibre electrodes are video microscopically recorded during charge/discharge conditions. In liquid electrolyte the total/reversible longitudinal expansion are found to be 0.85/0.8% while for the CF-SBE electrode the reversible expansion is found to be 0.6%. The fibre expansion in the CF-SBE electrode gives rise to residual strains which is demonstrated numerically. We expect that the utilized computational framework and experimental data open a route to develop high-performing, both mechanically and electrochemically, carbon fibre based battery electrode laminae for future lightweight structural components with energy storage ability.

1. Introduction

A viable route to create efficient lightweight multifunctional components for future electric vehicle and devices is to utilize structural materials with ability to storage energy (e.g. work as battery) [1–11]. One such solution exploits electrode laminae consisting of carbon fibres embedded in structural battery electrolyte (SBE). This type of material can be used in lithium-ion (Li-ion) based structural batteries, i.e. batteries with mechanical load-bearing capability [1,2,4–8,12–15], in electrochemical actuators [16], or in energy harvesting and strain sensing composites [17–19]. Due to the multifunctional character of such material, it offers a promising material choice for innovative future design of electric vehicles [6] and devices (e.g. laptops and phones) [20], as well as autonomous robotics [10], unmanned aerial vehicles [9,15] and satellites. In structural batteries, the carbon fibres can function as combined active electrode material, current collector and mechanical reinforcement. To allow for mechanical load transfer between the fibres, while facilitating Li-ions transport inside the electrode, the fibres are embedded in SBE [21,22]. The SBE consists of two phases: a solid phase which corresponds to a mechanically robust porous polymer network and a liquid phase which contains liquid electrolyte with Li-salt. The liquid phase in the porous polymer network enables ion transport between the electrodes, while the solid phase makes it possible to distribute mechanical loads. The SBE is a bi-continuous bi-phasic composite that consists of a porous polymer network (vinyl ester-based) with an open pore system saturated with the liquid electrolyte (1.0 M LiTf in

* Corresponding author.
E-mail address: david.carlstedt@chalmers.se (D. Carlstedt).
[1] Current address: Morrow Batteries, R&D Department, 4836 Arendal, Norway

https://doi.org/10.1016/j.compscitech.2022.109283
Received 10 October 2021; Received in revised form 17 January 2022; Accepted 18 January 2022
Available online 22 January 2022
0266-3538/© 2022 The Authors. Published by Elsevier Ltd. This is an open access article under the CC BY license (http://creativecommons.org/licenses/by/4.0/).

EC:PC), as schematically illustrated in Fig. 1a. The porous polymer network is formed via reaction induced phase-separation during the curing process, as described in Refs. [21,22]. It should be noted that the solid phase of the SBE in Fig. 1a corresponds to a numerically generated nano-structure, from Tu et al. [23], representing an idealized fine-scale geometry of the SBE (compare with SEM image in Fig. 1e). The characteristic pore size of the polymer network is roughly in the order of 50–200 nm [22].

The internal structure of an electrode made from carbon fibres embedded in SBE (referred to as CF-SBE electrode) and a conventional graphite electrode are shown schematically in Fig. 1a and b for comparison.

In the conventional graphite electrode, the electrode particles and conductive additives (e.g. carbon black) are adhered to a copper foil (current collector) using a polymer binder. Further, the porous structure of the electrode is soaked with a liquid electrolyte to allow for ion transport. Hence, the main differences of the CF-SBE electrode, as compared to the conventional graphite electrode, are essentially three: (i) The active electrode materials are fibres instead of particles; (ii) SBE is used instead of liquid electrolyte; (iii) The carbon fibres work as current collectors. This means that there is no need for polymeric binder, nor conductive additives, in the CF-SBE electrode (i.e. the upper surface of the fibre electrode in Fig. 1a does not need to be fully covered by metal foil). It should however be noted that the electrical conductivity of carbon fibres [24] is about three orders of magnitude lower than that of copper. Hence, the ohmic losses in the studied material will be significantly larger and will limit the electrode dimensions. In a recent study Johannisson et al. [25] demonstrate how screen-printing technology can be used to print current connectors (Fig. 1a) along carbon fibre based electrodes. This does not resolve the issue, but by utilizing certain printing pattern the electron transport along the fibres can be reduced/limited. Furthermore, it is noted that reported specific capacities and diffusion coefficients for certain types of carbon fibres are similar to those of commercially available graphite electrode materials [24,26,27]. The electrode design, i.e. electrode dimensions (thickness, width and length), transport properties of constituents, particle dimensions

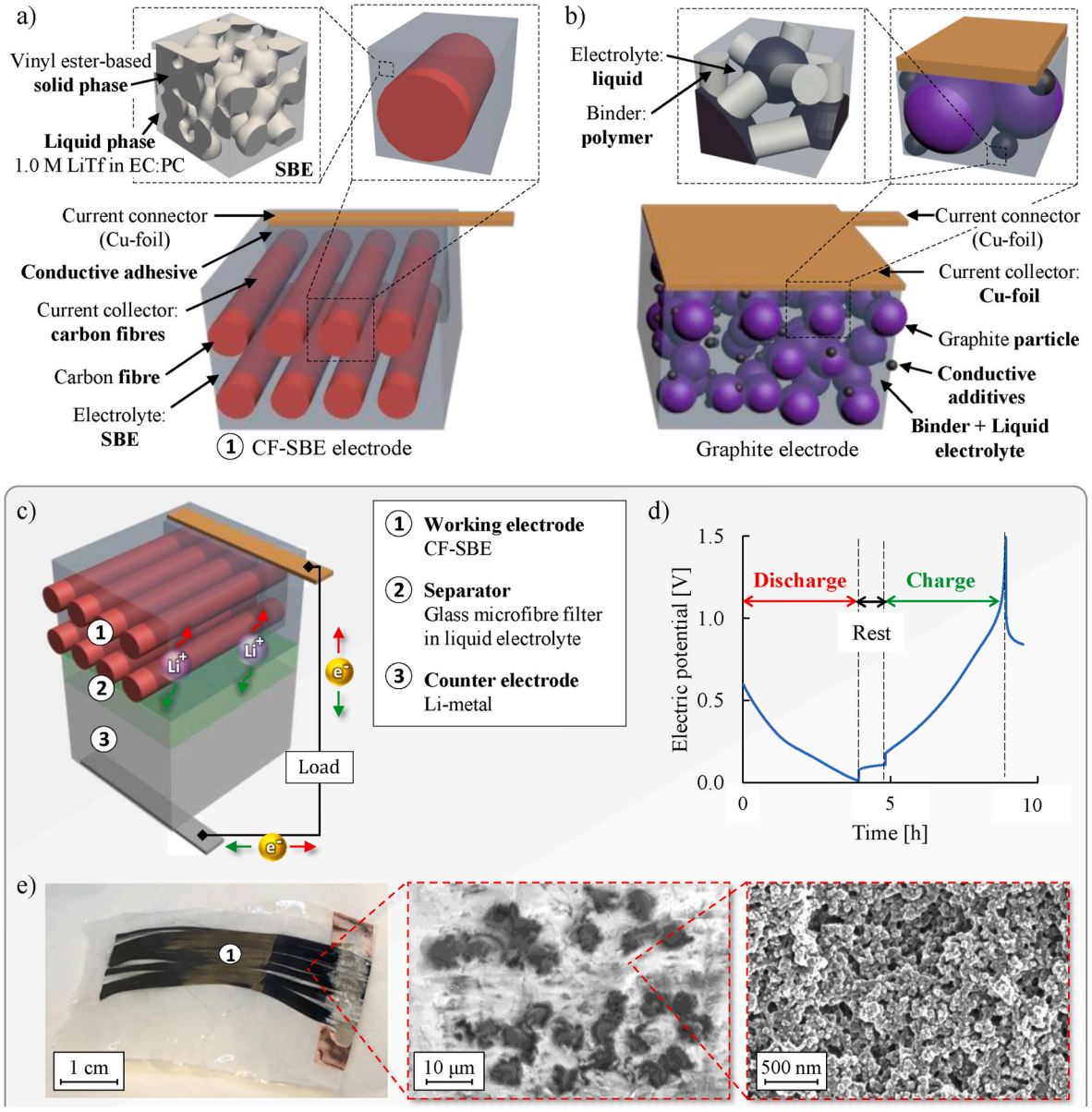

Fig. 1. Schematic illustration of (a) a CF-SBE electrode and (b) a conventional graphite electrode for comparison. The **bold text** represents the main differences between the two types of electrodes. (c) Schematic illustration of the studied CF-SBE electrode half-cell. (d) Convention for charge/discharge conditions. (e) Hierarchical structure: Photo of electrode (length scale: cm), SEM image of electrode cross-section (length scale: µm), SEM image of SBE (length scale: nm).

and distribution, etc. are known to have significant effect on the electrochemical performance of conventional battery electrodes [28–34]. Moreover, it is well known that the porosity and tortuosity of the electrode significantly influence the performance of the cell [35,36]. Due to the fact that the reported transport properties of the constituents in the CF-SBE electrode are inferior to those of the conventional electrode, these effects are expected to be even more pronounced for CF-SBE electrodes. For example, the electrical conductivity of carbon fibres [24] is significantly lower than that of copper, which is commonly used as current collectors in conventional graphite electrodes. Moreover, the ion conductivity of the SBE is in the order of 10^{-4} S cm^{-1} [21,22], whereas the conductivity of conventional liquid electrolytes is significantly higher, typically in the order of 10^{-2} S cm^{-1} [37] at room temperature. In addition, the carbon fibres undergo significant expansion when lithiated [16,38]. This means that the geometric and topological characteristics of the cell, i.e. thickness of the electrode, transportation properties of the constituents, etc., are expected to have significant effect on the electro-chemo-mechanical performance of CF-SBE electrodes. To the best of our knowledge, no study currently exists which investigates these effects in structural batteries.

In previous work by the authors, a novel computational modelling framework for studying the electro-chemo-mechanical properties of CF-SBE electrodes was developed [39]. Further, numerical studies of structural batteries have been performed previously [40–44]. However, in these studies no experimental validations were done. Only recently, Yin et al. [8] compared experimental and numerical results for modified carbon fibre electrodes in conventional liquid electrolyte (i.e. non-structural electrodes). The computational framework was based on the battery modelling scheme originally developed by Newman and co-workers [45–48] that presumes one-way coupling between the electrochemical and mechanical processes. To date, no study exists which combines a fully coupled computational framework with experimental data to characterize CF-SBE electrodes (i.e. structural electrodes).

In this paper, electrode laminae made from carbon fibres embedded in SBE are characterized with respect to their multifunctional (i.e.

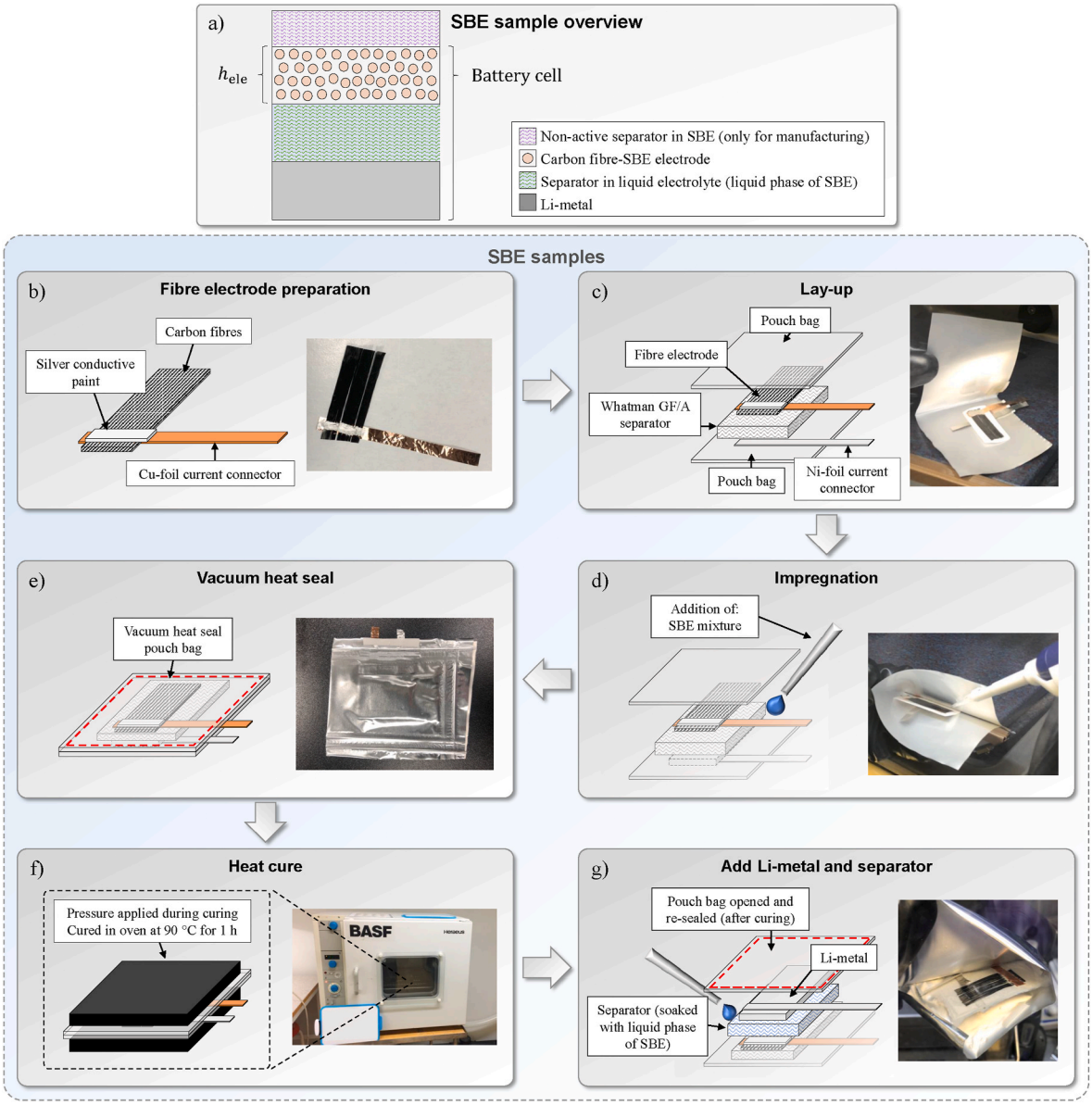

Fig. 2. (a) Schematic illustration of the SBE sample: CF-SBE electrodes with different electrode thickness (h_{ele}) vs. Li-metal, with a separator immersed in the liquid phase of SBE. (b)–(g) Fabrication process of the carbon fibre electrode half-cells utilizing SBE (SBE samples). The corresponding fabrication process of the reference (LE) samples are presented in Fig. S6, in Supplementary information.

combined electrochemical and mechanical) performance utilizing experimental and numerical techniques. We summarize existing material data from the literature and perform additional experiments in order to compare numerical predictions with experimental results. We utilize a previously developed computational modelling framework [39] and perform experimental and numerical studies on CF-SBE electrode half-cells (schematically illustrated in Fig. 1c). Two types of half-cells are studied: (i) one type utilizing CF-SBE electrodes (referred to as SBE samples, see Fig. 2a) and (ii) one type utilizing carbon fibre electrodes in conventional LP40 liquid electrolyte (referred to as LE samples). The latter samples are used as reference samples to evaluate the effects of embedding the fibres in the SBE. The electrode thickness and applied current are altered to study how the electrochemical performance of the cell is affected by these parameters. Further, Li-insertion induced longitudinal expansion of carbon fibre electrodes is measured *in situ* during charge/discharge processes using a Digital Image Correlation (DIC) technique, which is based on previous video microscopical electrode observations [49,50]. Expansion data for carbon fibres in liquid electrolyte (i.e. "free" expansion of fibres) and CF-SBE electrodes are recorded. Finally, the resulting residual strain levels, due to the partly constrained fibre deformation for the electrodes utilizing SBE, are evaluated numerically.

2. Material and methods

2.1. Materials

The carbon fibres are of the type intermediate modulus T800SC-12k-50C PAN-based manufactured by Toray Composite Materials America, Inc. The unidirectional fibre tows are spread to a width of approximately 15 mm by Oxeon AB (who kindly supplied the fibre tows). The thickness of the provided fibre tow is approximately 25 μm which corresponds to roughly 5 fibre diameters in the thickness direction and the linear tow weight is 0.52 g m^{-1}. These fibres have been characterized in terms of their multifunctional performance by e.g. Kjell et al. [24] and Fredi et al. [26]. The two phase SBE system is made from the following materials: (i) Solid polymer phase: Bisphenol A ethoxylate dimethacrylate (M_n: 540 g mol^{-1}) and 2,2′-Azobis(2-methylpropionitrile) (AIBN), supplied by Sartomer Europe; (ii) Liquid phase: Propylene carbonate (PC) (PC $\leq$ 99%, acid <10 ppm, H_2O <10 ppm), ethylene carbonate (EC) (99% anhydrous), and lithium trifluoromethanesulfonate (LiTf) (99.99%), purchased from Sigma Aldrich. The liquid electrolyte used for the reference (LE) samples is a Lithium hexafluorophosphate solution made from: 1.0 M $LiPF_6$ in EC:DMC 1:1 w/w (referred to as LP40), purchased from Sigma-Aldrich. The separator is made from Whatman glass microfibre filters (Whatman GF/A, 260 μm thick) purchased from Sigma Aldrich. The collectors are made from copper and nickel foil. The copper foil is adhered to the carbon fibres using PELCO® conductive silver paint. The collectors and the lithium metal foil are purchased from Sigma Aldrich. The utilized pouch laminate bag material is made from PET/Al/PE (i.e., an aluminium foil laminate with PET and PE polymer on either side) with thicknesses: 12 μm/9 μm/75 μm. All materials are used as received.

2.2. Structural battery half-cell preparation

The structural battery half-cells utilizing CF-SBE electrodes (i.e. SBE samples) are manufactured as schematically illustrated in Fig. 2. The fabrication process for the reference (LE) samples is presented in Supplementary Fig. S6 (for comparison). The fibre tow is cut in dimensions of 40 × 15 mm^2 which corresponds to approximately 21 mg of carbon fibres. A copper foil current collector is adhered to the carbon fibres using silver conductive paint to extract the current from the electrode (Fig. 2b). The samples are made from one, two or four fibre tows (dimensions 40 × 15 mm^2) placed on top of each other. The number of fibre tows are altered to evaluate the effects of increased electrode thickness h_{ele} (Fig. 2a). As combined counter and reference electrode Li-metal is utilized. To extract the current from the Li-metal a current collector made from Nickel foil is used. The separator is made from Whatman glass microfibre filter and is soaked in liquid electrolyte of the following type; (i) for SBE samples: liquid phase of the SBE and (ii) for LE samples: commercial liquid electrolyte. The carbon fibre tow and separator are arranged inside a pouch laminate bag, which is used to protect the electrochemical cell from air and moisture, as shown in Fig. 2c. For the reference samples utilizing liquid electrolyte, the Li-metal is added at this point (see Supplementary Fig. S6 for more information). The constituents in the pouch bag are then impregnated with either LP40 liquid electrolyte (LE samples) or SBE mixture (SBE samples), see Fig. 2d, before the pouch-bag is vacuum heat-sealed (Fig. 2e). For the LE samples, 1.0 M $LiPF_6$ in EC:DMC 1:1 w/w (LP40 Sigma-Aldrich) electrolyte is used and the manufacturing process is complete at this stage. For the SBE samples, the SBE mixture is prepared in accordance with the procedure described in Ref. [22]. The SBE mixture is made by mixing 40:60 wt % of (i) a liquid electrolyte solution made from 1.0 M LiTf in EC:PC 1:1 w/w (50:50 wt %) and (ii) monomer bisphenol A ethoxylate dimethacrylate and the thermal initiator, AIBN (1 wt % of the monomer weight). The properties of the SBE material are reported elsewhere [22]. The infused SBE mixture is thermally cured at 90 °C for 60 min (Fig. 2f). After curing the pouch bag is opened inside the glovebox and Li-metal foil and an additional separator, soaked in the liquid electrolyte solution for the SBE, are added on the side facing the carbon fibres (see Fig. 2g). The pouch bag is then re-sealed and ready for testing.

2.3. Galvanostatic cycling

The battery cells are tested running galvanostatic charge and discharge cycles. The cycling is performed using a Neware CT-4008-5V10mA-164 battery cycler. The samples are cycled between 0.01 V and 1.5 V using the following mass specific currents: 30, 60 and 120 mA g^{-1} relative to the mass of carbon fibres available in the battery cell. These currents correspond to equivalent C-rates of 0.19C, 0.5C, and 1.2C, with respect to the measured specific capacity of the reference sample (LE sample) made from one fibre tow. It should be noted that the C-rate is related to the (dis)charge time, where the corresponding (dis)charge times are 5.2 h, 2 h and 50 min. The cells are considered discharged at 0.01 V vs. Li/Li^+ and fully charged at 1.5 V vs. Li/Li^+. The electrochemical capacities of the tested samples are estimated as the electric charge delivered or received by the cell during the time for charge or discharge, respectively.

2.4. Mobility coefficients of the liquid phase of the SBE

The dynamic viscosity (Υ) of the liquid phase of the SBE is determined using a DMA 4500 M density meter from Anton Paar with a Lovis 2000 M micro-viscometer module. A steel ball (Ø = 1.5 mm, ρ = 7.70 g cm^{-3}) is used for dynamic viscosity measurements by the falling sphere method. The capillaries (Ø = 1.59 mm) are loaded inside the glove box.

The mobility coefficients η_α are then calculated from the Stokes–Einstein relation as

$$\eta_\alpha = \frac{1}{6\pi\Upsilon r_\alpha N_A} \tag{1}$$

where Υ is the dynamic viscosity of the fluid, r_α is the radius of the spherical particle for species α and N_A is the Avogadro constant.

2.5. Electrode expansion measurements

The longitudinal electrode expansion measurements are performed utilizing an optical *in situ* observation method described in detail in previous works [49,50]. This method uses Digital Image Correlation (DIC) to track the deformation of the specimen from video recorded

microscopical observations during electrochemical cycling.

2.5.1. Cell assembly

The electrodes used for the expansion measurements are manufactured in accordance with the procedure described in Section 2.2. The electrode dimensions for these samples are adjusted in order to fit the windowed test cell. Hence, the fibre tow is cut in dimensions of approximately 5 × 1.5 mm^2 which corresponds to approximately 0.26 mg of carbon fibres. To ensure a sufficient lithiation of the carbon fibre electrode a plate of Li-metal is used as combined counter and reference electrode. The fibre electrode and Li-metal is separated by a 220 μm-thick separator made of polypropylene fibre/polyethylene membrane (EL-Cell GmbH, FS-5P). The fibre-separator-Li-metal stack is then placed (under argon atmosphere) in a test cell with an optical window (EL-Cell GmbH, ECC-Opto-Advanced) with the fibre electrode being visible through the window. Finally, approximately 100 μl 1.0 M $LiPF_6$ in EC:PC 1:1 w/w electrolyte solution (Sigma-Aldrich) is added.

2.5.2. Measurement setup

Electrical monitoring and measurement of currents and voltages are performed with the potentiostat Ivium OctoStat 30. For charging as well as discharging a constant-current-constant-voltage (CCCV) cycling mode, followed by a 2 h rest time, is used. The cells are cycled in the voltage limits of 0.01 mV and 1.5 V and the initial currents in the CC modes are set to 20 μA which corresponds to approximately 77 mA g^{-1} of fibres. The cut-off current is set to 2 μA. The camera setup consists of the USB3-camera mvBlueFox3-2064C, the macro lens MV-OMC303-OE (both MatrixVision) and an illumination ring with LEDs. Images are recorded every 4 min.

2.5.3. Post-processing

Post-processing of measurement data to estimate the longitudinal electrode expansion is performed within the MATLAB software environment. Here, only major steps are addressed for simplicity. A detailed explanation is given in Supplementary information. The length of the fibre electrodes are obtain from a pixel-length-conversion using the diameter of the window (10 mm) as reference object. To separate the dark electrode from the bright underlying separator, the image information is transformed from the RGB color space to the HSV representation to use the brightness channel as boundary indicator of the electrode. Since the latter is a step-like function, its derivative yields a maximum. The real space coordinate of this maximum is identified as electrode boundary. The total longitudinal expansion of the electrode is obtained from the boundaries on both ends. The relative expansion is given by the ratio of the longitudinal expansion and the initial length of the fibres.

2.6. Scanning Electron Microscopy (SEM)

The microstructure of the CF-SBE electrodes are studied using Scanning Electron Microscopy (SEM). The electrodes are broken and dried (24 h in 50 °C vacuum) prior to coating with palladium using a Emitech K500X sputter coater for 30 s in argon atmosphere. The SEM images are produced with a Zeiss Leo Ultra 55 field emission gun scanning electron microscope with an accelerating voltage of 2 kV.

2.7. Tensile testing (mechanical performance)

The tensile tests are conducted in accordance with the experimental procedure described in Ref. [1]. A Deben 2 kN tensile stage microtester is used under displacement control at a rate of 0.1 mm min^{-1}. The tensile tests are performed in the fibre direction to measure the elastic moduli of the CF-SBE electrode laminae. The electrodes are manufactured in accordance with the procedure described in Section 2.2. This means that the supporting (non-active) separator in Fig. 2a is included in the specimen. For comparison, additional samples are prepared containing only the separator embedded in SBE. The dimensions of the test specimens are approximately 30 × 3 mm^2 (length × width). The slender specimens are produced by carefully cutting the electrodes to the desired dimensions. The tensile tests are preformed on three samples per specimen and are conducted on pristine electrodes (i.e. no electrochemical cycling is performed prior to the test).

2.8. Model specifications

The utilized computational framework was developed in a previous study by the authors [39]. Compared with previous work, the model geometry now includes the separator phase while accounting for its effective properties. Moreover, the electrode thickness and fibre volume fraction are based on experimental data. A detailed description of the computational framework, including time-continuous strong format and modelling assumptions for the individual domains, interfaces and boundaries, etc., is provided in Supplementary information. The framework is based on some general modelling assumptions. Firstly, isothermal condition is assumed. Further, all material phases are assumed linear elastic (small deformations), linked to the mechanical response. However, material nonlinearities are present in the electrochemical relations. Self-weight is ignored, i.e. no body load is present. Finally, any piezoelectric effect is ignored, which means (in particular) that stresses do not depend explicitly on the electric field.

In this study, the following model approximations for the chemical potential of Li in the carbon fibres are used to evaluate their respective correlation with the experimental results:

$$\textbf{Model1}: \mu_{\mathrm{Li}} = -c_{\mathrm{Li},\ \max}^{-1}\boldsymbol{\alpha}^{\mathrm{ch}} : \boldsymbol{\sigma}(\boldsymbol{\varepsilon}, c_{\mathrm{Li}}) + \mu_{\mathrm{Li}}^{0} + R\theta_0 log(f_{\mathrm{Li}}(\widetilde{c}_{\mathrm{Li}})\widetilde{c}_{\mathrm{Li}}) \tag{2a}$$

$$\textbf{Model2}: \mu_{\mathrm{Li}} = -c_{\mathrm{Li},\ \max}^{-1}\boldsymbol{\alpha}^{\mathrm{ch}} : \boldsymbol{\sigma}(\boldsymbol{\varepsilon}, c_{\mathrm{Li}}) + \mu_{\mathrm{Li}}^{0} + h_0[1-2\widetilde{c}_{\mathrm{Li}}] + R\theta_0 log(f_{\mathrm{Li}}(\widetilde{c}_{\mathrm{Li}})\widetilde{c}_{\mathrm{Li}}) \tag{2b}$$

$$\textbf{Model3}: \mu_{\mathrm{Li}} = -c_{\mathrm{Li},\ \max}^{-1}\boldsymbol{\alpha}^{\mathrm{ch}} : \boldsymbol{\sigma}(\boldsymbol{\varepsilon}, c_{\mathrm{Li}}) + \lambda(\widetilde{c}_{\mathrm{Li}}) \tag{2c}$$

Here we define the normalised mass concentration of Li in the fibre as $\widetilde{c}_{\mathrm{Li}} = \frac{c_{\mathrm{Li}}}{c_{\mathrm{Li},\ \max}}$, where c_{Li} is the mass concentration (molarity) and $c_{\mathrm{Li,\ max}}$ is the assumed maximum concentration of Li in the carbon fibre. Further, $\boldsymbol{\alpha}^{\mathrm{ch}}$ is a second order tensor containing the coefficients of the insertion induced expansion of the fibres and $\boldsymbol{\sigma}$ is the (symmetric) stress tensor which is a function of the (small) strain tensor $\boldsymbol{\varepsilon}[\boldsymbol{u}]$, expressed as a linear operator of the displacement field $\boldsymbol{u}$. Finally, μ_{Li}^{0} is the reference chemical potential, R is the gas constant and θ_0 is the reference temperature.

In Eq. (2a), the general/idealized expression for the chemical potential is utilized as described in Ref. [39]. In Eq. (2b), the enthalpic term $h_0[1-2\widetilde{c}_{\mathrm{Li}}]$ is added to account for particle-hole repulsion that cause immiscibility of the Li and its host [51]. This is in line with the expression for intercalation compounds proposed and utilized by Doyle et al. [46]. Further, in Eq. (2c), $\lambda(\widetilde{c}_{\mathrm{Li}})$ represents an arbitrary regression model which is approximated by fitting the function to experimental data. The activity coefficient f_{Li} in Eqs. (2a)-(2b) is chosen in accordance with the definition for an ideal solid solution of non-interacting particles on a lattice in Bazant [52]: $f_{\mathrm{Li}}(\widetilde{c}_{\mathrm{Li}}) = \frac{1}{1-\widetilde{c}_{\mathrm{Li}}}$. The reference chemical potential for the Li atoms in the fibre is denoted μ_{Li}^{0}. It should be noted f_{Li} can be defined in different ways depending on the assumed interaction between the ions and the host material. For example, extended/refined constitutive models, as compared with Model 1 and 2, for intercalation compounds are available in the literature, see e.g. Ref. [46]. However, the basic understanding of the physics behind the insertion mechanisms of Li-ion into carbon fibres is still lacking [26]. Finally, it should be noted that utilizing an arbitrary regression model (i.e. Model 3), allows for better agreement with experiments but lack generality. This type of approximation is however commonly used in the electro-chemistry literature (defined in terms of the open-circuit potential), see e.g. Refs.

[8,53].

3. Results and discussion

3.1. Microstructure of CF-SBE electrode

The hierarchical structure of the studied CF-SBE electrode, illustrating the relevant length scales, is shown in Fig. 1e. The typical radius of the fibres is 2.5 μm and the distribution of the fibres depends on the fibre volume fraction, manufacturing process, etc. Further, the typical pore size of the SBE is in the order of 100 nm and the porosity/pore size depends on e.g. mixing ratio of monomer to liquid electrolyte, type of monomer, etc. The properties of the SBE can be altered by modifying the composition of the polymer/electrolyte mixture (e.g. using different monomers or mixing ratios of monomer to electrolyte), see Refs. [21,22].

The microstructure of the CF-SBE electrode is studied using SEM. A cross-section view of a CF-SBE electrode is shown in Fig. 3a. Zones with high SBE and fibre content, respectively, are identified. However, these zones are limited in size and the appearance of the evaluated cross-sections motivate the idealized model representation shown in Fig. 3d and e. Moreover, porous CF-SBE interfaces (Fig. 3b) and SBE residue on carbon fibres (Fig. 3c) are found after fracture (as reported in Ref. [5]). This indicates that the current exchange (liquid phase of SBE access fibres) and mechanical load transfer (solid phase of SBE access fibres) can occur simultaneously along the interfaces within the electrode. It should be noted that the SBE appears to be isotropic at the studied/resolved scale (i.e. micro-scale). However, at the immediate vicinity of the fibres further evaluation is needed.

The conceptual/idealized model representation of the studied half-cell is presented in Fig. 3e. The model represents an idealized repeatable unit in the horizontal direction where the height of the unit corresponds to the height of the cell (Fig. 3d) and is utilized in the computational model (described in Section 2.8 and in Supplementary information). The introduced notation is defined in Supplementary information. The electrode thicknesses (h_{ele}), thickness of the separator (h_{sep}) and fibre volume fractions (Fig. 3d) are either estimated based on image analysis of SEM images of the cross-section or assumed based on material data from the supplier. For example, the fibre volume fraction of the CF-SBE electrode is estimated based on the complete cross-section image in Fig. 3d. Given the distinct color difference between the fibres and SBE, this is simply done by increasing the contrast and comparing the percentage of pixels in the respective zones (fibres/SBE). In the idealized model the counter/reference electrode (i.e. the Li-metal) is simply replaced by a collector at boundary Γ_+.

3.2. Material properties of constituents

The complete set of collected material data used in the analysis is available in Supplementary Table S3. Further, details regarding the origin and derivation of the individual parameters are presented in Supplementary information. Here we present the experimental data for the measured equilibrium potential of the utilized carbon fibres and mobilities of the ions in the liquid phase of the SBE (as complement to the collected data from literature) to allow for comparing numerical and experimental results for the studied half-cell.

The measured electric/electrode potential during lithiation (i.e. discharge in Fig. 1d) of the carbon fibre electrode utilizing LP40 liquid electrolyte (LE sample in Fig. 2a) for an applied current of 15 mA g^{-1} of carbon fibres is presented in Fig. 3f. The results are used for approximating a fitting function $\lambda(\widetilde{c}_{Li})$ in Eq. (2c), utilized in the computational model. It should be noted that the measured potential is only an approximation of the equilibrium potential of the carbon fibres. However, the measured electric potential is in close agreement with previous reported data [27,38]. The specific capacity measured at this applied current is approximately 240 mAh g^{-1} (defined with respect to the mass of the carbon fibres) with a discharge time of approximately 13 h. This is in the same range as previous measurements [24,38]. The measurement data are provided in Supplementary Table S1.

The mobility coefficient of Li in the liquid phase of the SBE (i.e. 1M LiTf EC:PC) is found to be $\eta_{Li} = 1.30 \cdot 10^{-13}$ $m^2 mol\ s^{-1} J^{-1}$. Further, the mobility coefficient of the triflate is found to be $\eta_{Tf} = 3.82 \cdot 10^{-14}$ $m^2 mol\ s^{-1} J^{-1}$ (Fig. 3g). It should be noted that the Stokes-Einstein relation (Eq. (1)) is only valid for spherical particles; however, in here we assume that Tf is spherical in order to get an approximation to its mobility coefficients. The radii used are 0.090 and 0.307 nm for Li and Tf, respectively, based on the calculations by Okan et al. [54]. Even though this is a rough approximation, our values are in the same order of magnitude as those obtained by advanced techniques such as Li field-gradient NMR [55]. The dynamic viscosity of the liquid phase of the SBE at room temperature was measured to be $\Upsilon' = 7.51$ mPas. For completeness, additional measurement data on the dynamic viscosity and ion conductivity as function of temperature are provided in Supplementary Fig. S3. Details regarding the experimental procedure for estimating the ion conductivity are also included in Supplementary information.

3.3. Mechanical performance of CF-SBE electrode

The mechanical performance of the CF-SBE electrode is assessed in terms of the elastic modulus of the composite laminate in the fibre direction. The force versus displacement curves for the case of tensile load applied in the fibre direction for the CF-SBE electrode with $h_{ele} = 100$ μm (including the supporting separator from manufacture), and the corresponding separator embedded in SBE (for comparison), are presented in Fig. S5 in the Supplementary information. The elastic modulus of the CF-SBE electrode lamina in the longitudinal direction is found to be approximately 57 GPa. Based on the Voigt's assumption of iso-strain in the fibre direction, the fibre volume fraction is estimated to be approximately 20%. This is in agreement with the estimated value from image analysis of the cross-section, described in Section 3.1. Further, the measured value is also in agreement with previous measurements on similar material systems [1,5]. Finally, the stiffness of the separator embedded in SBE is found to be approximately 0.83 GPa. This is only a slight increase in elastic modulus as compared with the pure SBE system (approximately 0.54 GPa [21,22]). Hence, it is clear that the fibres are decisive for the elastic modulus in the fibre direction. It should be noted that strength values and stiffness in the transverse direction are not reported due limitations in the sample preparation process.

3.4. Electrochemical performance of CF-SBE electrode half-cell

Fig. 4 shows experimental results from galvanostatic cycling of a CF-SBE electrode half-cell (shown in Fig. 4a) with an electrode thickness of $h_{ele} = 50$ μm.

Fig. 4b shows the typical charge/discharge voltage profiles of the half-cell at different applied mass specific currents defined with respect to the mass of carbon fibres available in the electrode. These profiles indicate a stable charge/discharge process at different mass specific currents. Moreover, Fig. 4c shows the specific capacity over continuous cycling at different applied currents. Finally, in Fig. 4d the specific capacity is plotted against the mass specific current (with respect to the mass of the fibres) for the CF-SBE electrode (SBE) and the carbon fibre electrode in conventional LP40 liquid electrolyte (LE), i.e. LE sample, for comparison. At applied currents 30 and 120 mA g^{-1} of carbon fibres, the relative reduction in the specific capacities for the CF-SBE electrode, in comparison with the half-cell utilizing liquid electrolyte, are approximately 25% and 54%, respectively. Hence, it is evident that the inferior transport properties of the SBE impair the electrochemical performance of the cell, in particular at high currents. It should be noted that the results presented in Fig. 4d are based on single specimens (hence, no data scatter is included). The trends are in agreement with previous

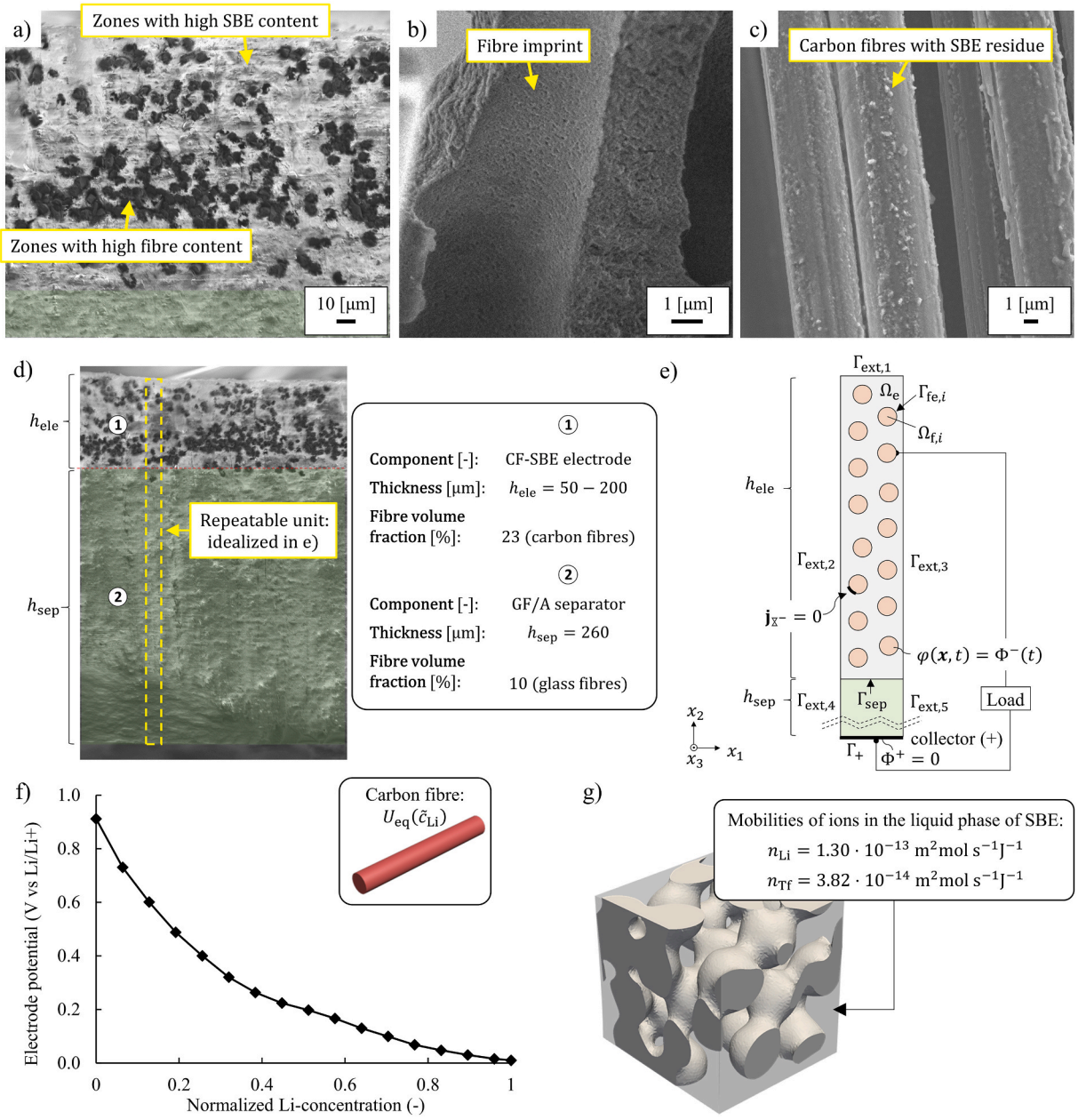

Fig. 3. SEM-images of: (a) The cross-section of a CF-SBE electrode; (b) Fibre imprint. The fibre-SBE interface is found to be porous; (c) Carbon fibres with SBE residue. (d) SEM image of CF-SBE electrode half-cell cross-section. (e) Conceptual/idealized model representation of the half-cell. (f) Measured electric potential (during lithiation) of carbon fibre electrode in liquid electrolyte for an applied current of 15 mA g^{-1} of fibres. (g) Measured mobility coefficients of the ions in the liquid phase of the SBE (3D-image of SBE from Ref. [23]).

measurement [5,21,22,24]. The measured specific capacity (at low applied current) for the carbon fibre half-cell in liquid electrolyte presented in Figure 4d, is also in close agreement with previous measurement reported by e.g. Kjell et al. [24]. Further, compared with previous studies on similar types of carbon fibres in liquid electrolyte, e.g. Refs. [8,38], the measured specific capacity is slightly lower. This is thought to be linked to the experimental design (e.g. choice of electrolyte and separator) and electro-chemical performance of the selected fibres, see e.g. Ref. [56]. Hence, different carbon fibres can be used to attain improved electro-chemical performance. Moreover, the specific capacities measured for the CF-SBE electrode half-cell are similar to those previously reported by e.g. Johannisson et al. [5] and Schneider et al. [22]. In the former, a slight difference is noted which is assumed to be associated with a difference in applied mass specific current (results are only reported for an applied current of 18.6 mA g^{-1} of fibres) and fibre/SBE content. Furthermore, in Ref. [5] it was shown that the elastic moduli of the studied material are retained after electrochemical cycling. Moreover, in Ref. [22] the stability of the studied system was demonstrated over 40 repeated charge/discharge cycles. Finally, it should also be noted that the utilized separator influence the performance (e.g. the specific capacities in Fig. 4d). For example, the separator thickness, wettability, etc., significantly impair the electrochemical performance. Hence, some of the losses associated with the reported capacities are due to the separator. However, these losses are assumed to be the same for the different samples (i.e. SBE vs. LE). In the current study, a thick and highly porous separator is used. Thinner separators, e.g. made from a thin layer of SBE, are expected to improve the performance significantly.

In Fig. 5a and b, the measured and the predicted (using the computational framework) voltage profiles of the CF-SBE half-cell

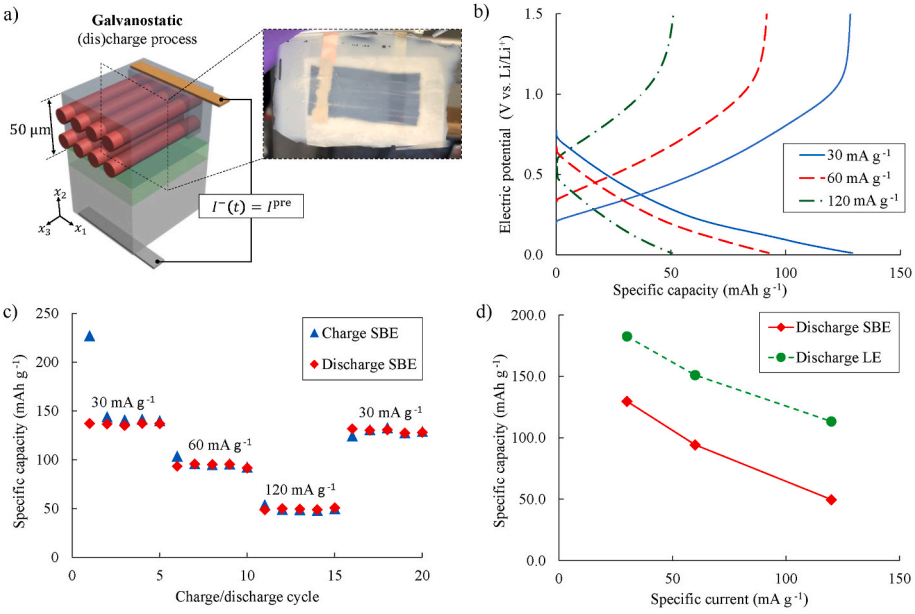

Fig. 4. (a) Galvanostatic cycling of half-cell with CF-SBE electrode thickness: h_{ele} = 50 µm (SBE sample in Fig. 2a). (b) Voltage profiles at different mass specific currents. (c) Specific capacity at different mass specific currents. (d) Specific capacity (measured during discharge) versus mass specific current for the CF-SBE electrode (SBE) and a carbon fibre electrode in LP40 liquid electrolyte (LE) for comparison. The specific capacities and mass specific currents are defined with respect to the mass of carbon fibres in the electrode.

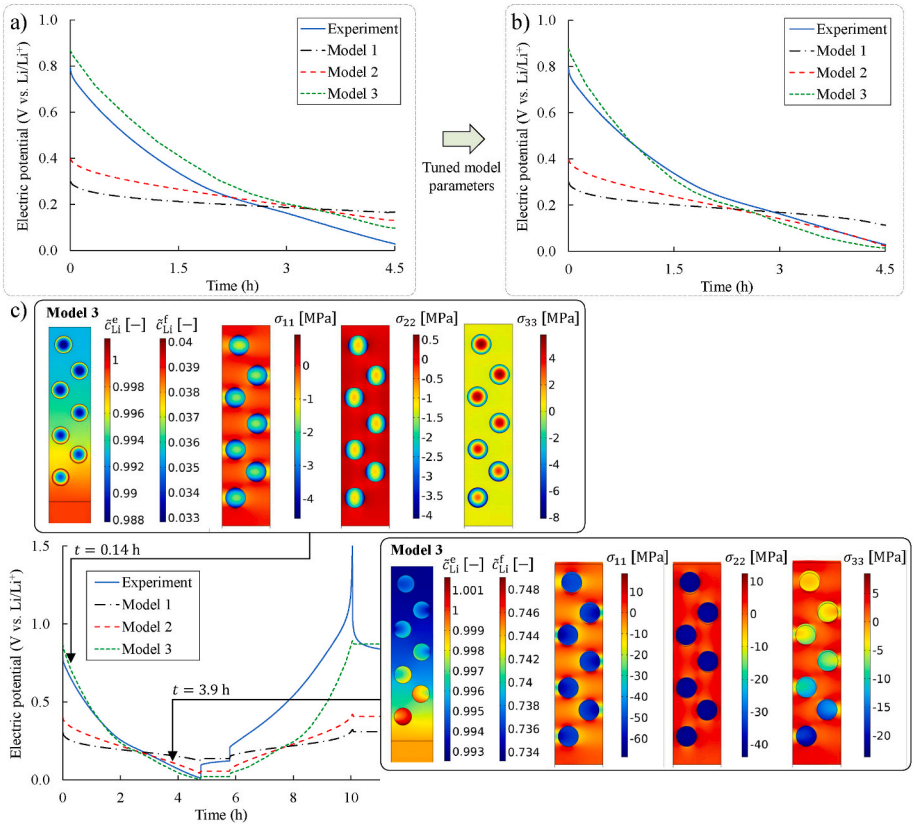

Fig. 5. Model predictions and experimental data for the electric potential of the CF-SBE half-cell (electrode thickness of 50 µm), during galvanostatic discharge at applied current 30 mA g^{-1} of fibres: (a) The specific capacity C_f (and corresponding $c_{Li,\,max}$) is based on the reference sample (i.e. LE sample); (b) $c_{Li,\,max}$ is redefined based on the measured C_f for the given CF-SBE electrode half-cell. (c) Measured and predicted electric potentials during a complete discharge/charge cycle, and predicted (by Model 3) normalised Li-concentration in the fibres ($\tilde{c}^f_{Li}$) and SBE ($\tilde{c}^e_{Li}$) and the stress fields (σ_{ii}), at two time instances.

during a single discharge cycle are presented.

During discharge, the applied current is set to 30 mA g^{-1} of carbon fibres. In Fig. 5a, the specific capacity C_f (and corresponding $c_{Li,\,max}$)[2] is based on the reference sample using a carbon fibre electrode in liquid electrolyte (i.e. LE sample). It is possible to improve the model approximations by fitting/adjusting model parameters (which is common in literature, see e.g. Ref. [8]). For example, the maximum Li-concentration ($c_{Li,\,max}$) in the fibres can be tuned based on experimental data for the specific capacity for the given cell. In Fig. 5b, the numerical predictions are shown for the case when $c_{Li,\,max}$ is redefined based on the measured specific capacity for the studied CF-SBE electrode

[2] The maximum Li-concentration in the fibres is estimated as $c_{Li,\,max} = C^f \rho^f 3600/F$, where C^f is the assumed specific capacity and ρ is the fibre density.

half-cell (instead of the reference sample in liquid electrolyte).[3] This means that $\widetilde{c}_{\mathrm{Li}}$ now varies between 0 and 1 during the discharge cycle. In this case, Model 3 gives a good approximation as the specific capacity of the cell has been fitted to experimental data. This however requires new data (i.e. specific capacities) for different cell designs and applied currents in order to achieve good agreement between numerical and experimental results. Additional information regarding tuning of the model parameters is provided in Supplementary information.

To further demonstrate the capabilities of the computational framework, the measured and predicted electric potential for a complete discharge and charge cycle is presented in Fig. 5c. After each individual charge/discharge cycle the cell is allowed to rest for 1 h. During this time the applied current is set to zero. It is clear that the relaxation behaviour of electric potential is not fully captured by any of the Models due to model simplifications associated with e.g. interface conditions, material properties, etc. However, the overall behaviour of the cell is well taken for all Models given their simplistic nature and the relatively low number of required input data, in particular for Model 1 (in comparison with e.g. Refs. [8,46]). Moreover, predicted normalised Li-concentrations ($\widetilde{c}_{\mathrm{Li}}$) and stress fields ($\sigma_{ii}$) at two time instances during the discharge process are shown in Fig. 5c (for Model 3).[4] These results demonstrate that the framework is able to capture the development of mechanical stresses and strains during electrochemical cycling. In the early stage of the discharge process, the stresses are low due to the assumed stress free state of the material for $\widetilde{c}_{\mathrm{Li}} = 0$ in the fibre. As the half-cell discharge (during which Li-ions are inserted in the carbon fibres), the stresses increase as a result of the fibre expanding with increased Li-concentration. It should be noted that to accurately resolve the stress state, the non-linear (mechanical) material behaviour of the SBE need to be accounted for, e.g. linked to validity of small strain kinematics, stress relaxation, etc. However, it is clear that the provided framework is able to predict strain levels associated with insertion induced expansion/shrinkage of the fibres within the regime of small deformations and linear elastic material response. Further, due to the assumed stress/strain condition in the x_3 − direction (described in Supplementary information), i.e. along the fibres, the three-dimensional stress state is captured even though the FE-analysis is two-dimensional. Finally, it should be noted that the modelling framework is able to account for the highly anisotropic (transverse isotropic) mechanical character of the carbon fibres.

3.5. Effects of electrode thickness on electrochemical performance

Specific capacities for half-cells utilizing CF-SBE electrodes (SBE in Fig. 6), with different electrode thicknesses (shown schematically in Fig. 6a), at different mass specific currents are presented in Fig. 6b–d. The specific capacities of reference samples, utilizing carbon fibre electrodes with the equivalent mass of carbon fibres in LP40 liquid electrolyte (LE in Fig. 6), are also included for comparison. The specific capacities and applied mass specific currents are defined based on the mass of carbon fibres in the battery cell. The tested half-cells demonstrate stable charge/discharge processes and good capacity retention over the repeated cycles for all evaluated electrode thicknesses.

However, it is evident that the electrode thickness greatly affects the electrochemical performance. For example, increasing the electrode thickness of the studied CF-SBE electrode from 50 μm to 200 μm results in a reduction in specific capacity of approximately 70/95% for an applied current of 30/120 mA g^{-1} of fibres, respectively (Fig. 6b and d). Further, for a CF-SBE electrode with a thickness of 50 μm, the specific capacity at 30 mA g^{-1} of fibres is approximately 130 mAh g^{-1} (Fig. 6b). This is roughly 17% lower compared with the reference sample utilizing a carbon fibre electrode (with the same amount of fibres) in liquid electrolyte. For a CF-SBE electrode thickness of 200 μm, the specific capacity is approximately 38 mAh g^{-1} at 30 mA g^{-1} of fibres which is roughly 75% lower compared with the equivalent cell utilizing liquid electrolyte. This reduction, associated with the introduction of the SBE, is further increased at higher currents. In the case of an electrode thickness of 200 μm, the reduction in specific capacity for an applied current of 120 mA g^{-1} of fibres is as large as approximately 97% (Discharge LE: 77 mAh g^{-1} vs. Discharge SBE: 2.6 mAh g^{-1} in Fig. 6d). Moreover, it is noted that the reduction in the specific capacities for the SBE samples are approximately proportional to the electrode thickness. For example, for the SBE samples the reduction in capacity at low current are approximately 50% and 70% for the electrode thicknesses 100 and 200 μm, respectively, compared the case of 50 μm. For the LE samples, these reductions are only 0% and 10%. Hence, the electrochemical performance of CF-SBE electrodes is highly affected by the properties of the SBE, manufacturing procedure, etc., and significant improvement in performance can be achieved by utilizing thin electrodes or by improving the transport properties of the SBE (as for conventional battery electrodes [28–30]). The latter can either be achieved by improving the transport properties of the liquid phase of the SBE or by tailoring the pore structure of the SBE [23,57]. It should be noted that all tested cells are able to store and deliver electrical energy for the evaluated mass specific currents. Further, the Coulombic efficiencies for the samples in Figs. 5–6 are provided in Supplementary Fig. S4.

3.6. Fibre electrode expansion during electrochemical cycling

The fibre expansion, in the fibre direction, due to Li-insertion is video microscopically recorded *in situ*. Elongation data from a carbon fibre electrode in liquid electrolyte, cycled under CCCV conditions, are presented in Fig. 7a and b.

The total elongation of the specimen is estimated as the sum of the longitudinal fibre expansions at the two sides relative to the connection point between the fibres and the metal foil connector (Fig. 7a). The total longitudinal fibre expansion is found to be approximately 0.85% with a reversible longitudinal expansion of 0.8% (Fig. 7b). Hence, the irreversible expansion, associated with trapped Li-ions, SEI formation, etc. is approximately 0.05% and appears to mainly occur during the first charge/discharge cycle. These results are in agreement with previous measurements done by Jaqcues et al. [38] and Duan et al. [58]. Further, it is evident that the fibre elongation is linked to the applied electric current. For the galvanostatic phase (CC-phase), a close to linear elongation curve is recorded during (dis)charge while during the potentiostatic phase (CV-phase), utilized at the end of the individual charge/discharge cycles, the relative increase in elongation reduce with reduced current. In Fig. 7c and d, experimental results from the elongation measurements of a CF-SBE electrode lamina (i.e. SBE sample in Fig. 2a) are presented. The measured elongation curve of the CF-SBE electrode is shown in Fig. 7d. The reversible longitudinal electrode expansion is found to be approximately 0.6%. It seems that the SBE does not significantly influence the fibre expansion/shrinkage during (dis) charge. Further, the reduction in elongation, in comparison with the reference sample in liquid electrolyte, is assumed to be partly associated with the reduced specific capacity caused by the introduction of the SBE. It should be noted that the electrode appears to shrink at the beginning of the first discharge cycle (Fig. 7d). This is assumed to be an artifact associated with issues related with image contrasts for the measurements of the CF-SBE electrode. It should also be noted that some portion of the fibre electrode appears to lose contact to the current collector due to the (electro-chemically unstable) silver glue. This is assumed to result in the small offset visible in the elongation curve in Fig. 7d (i.e. for the CF-SBE electrode), comparing the first and subsequent charge/discharge cycles. The total longitudinal expansion is therefore not reported.

[3] It should be noted that $\alpha_{\perp}^{\mathrm{ch}}$ and $\alpha_{\parallel}^{\mathrm{ch}}$ are linked to the assumed maximum Li-concentration/specific capacity and should therefore be adjusted in accordance with the capacity to avoid unrealistically large expansion/shrinkage of the fibres.

[4] Negligible difference in $\widetilde{c}_{\mathrm{Li}}$ and σ_{ii} are found between the three models.

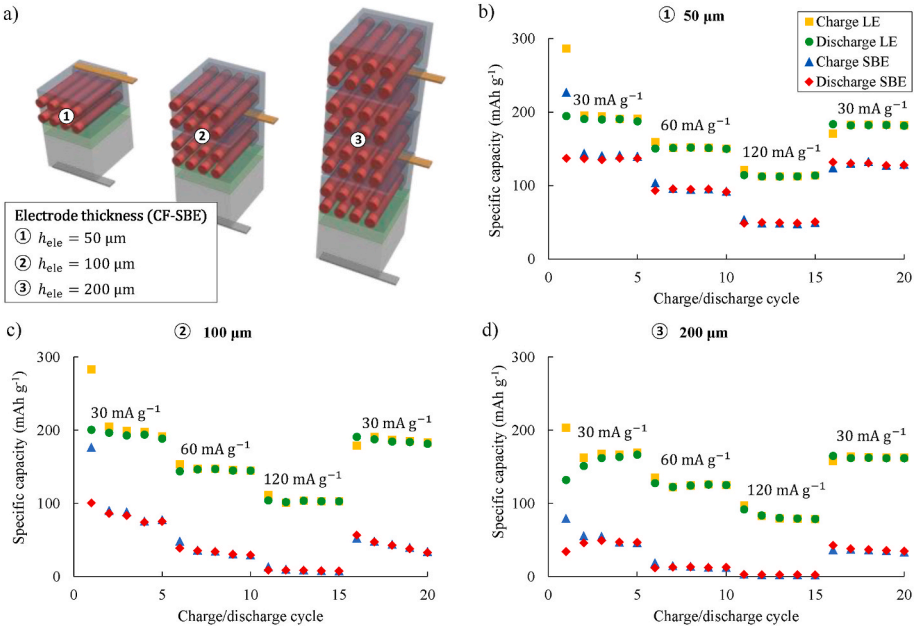

Fig. 6. (a) Schematic illustration of the three evaluated half-cells with different electrode thicknesses. (b)–(d) Measured specific capacities for different applied currents, for half-cells utilizing CF-SBE electrodes (SBE) with thicknesses 50 µm, 100 µm and 200 µm, respectively, and half-cells with equivalent mass of carbon fibres but instead soaked with LP40 liquid electrolyte (LE) for comparison. The specific capacities and applied mass specific currents are defined based on the mass of carbon fibres in the battery cell.

Moreover, the silver glue is assumed to influence the measured capacities [59]. However, this effect is assumed to be small given the fibre to silver content in the samples utilized to evaluate the specific capacities (Figs. 4 and 6). Finally, this is also thought to be the reason for the minor irregularities in the current versus time curves in Fig. 7b and d.

It should also be noted that the color of the fibres changes when lithiated (see e.g. Fig. 7a). At virgin state the fibres are black while at the lithated state the fibres turn black/red. The color change is related to the coordination of Li-atoms with the carbon-atoms in the fibre (see e.g. Ref. [60]). Since this process of lithium insertion is different from common graphite electrodes, no golden color can be seen in a fully lithiated carbon fibre electrode. Further, the color change appears to occur equally along the fibres which reveals that the electrode is lithiated simultaneously.

Videos of the carbon fibre electrode in liquid electrolyte (Fig. 7a) and the CF-SBE electrode (Fig. 7c) elongation during electrochemical cycling are provided in Supplementary information. The free expansion of the carbon fibres during lithiation is measured in liquid electrolyte. Stresses in the structural (CF-SBE) electrode evolve during lithiation as this free expansion is restricted by the surrounding SBE. To predict the stress state in the CF-SBE electrode the free (in LE) as well as the constrained (in SBE) expansions are measured. In addition to the longitudinal expansion, the CF-SBE electrode will expand in the transverse direction. The total transverse expansion of electrode lamina is estimated using the classical analytical model for thermal expansion developed by Scharpery [61], details are provided in Supplementary information. Based on the expected radial expansion of the carbon fibres measured by Duan et al. [58], the predicted transverse expansion of the specimen is around 0.6%, which for the given specimen dimensions correspond to a displacement of roughly 3–6 μm. Hence, this expansion is hardly visible in the video, and given the resolution of the utilized camera (approximately 3.5 μm/pixel), the displacement in the transverse direction cannot be measured using the current set-up.

The predicted numerical response, using Model 3, of the mechanical strain and stress fields (ε_{ii}, σ_{ii}) in the CF-SBE electrode at the lithiated state are presented in Fig. 7e. For the numerical simulation, the longitudinal fibre expansion (i.e. in x_3-direction) is based on the measured reversible elongation of the CF-SBE electrode and the transverse/radial fibre expansion is based on measurements by Duan et al. [58]. It is evident that the fibre expansion give rise to residual strains (Fig. 7e) which the constituents need to be able to cope with to avoid damage/degradation. Further, it can be seen that the estimated tensile stress components (Fig. 7e) in the matrix are as high as 10–15 MPa in some areas. This range can be compared with the average apparent transverse tensile strength of carbon fibre reinforce SBEs (11–17 MPa) measured by Xu et al. [62]. The magnitude of the strains and stresses depend on several factors e.g. material properties of constituents, assumed boundary conditions (discussed in Ref. [39]), etc. Further, in the case of a non-symmetric laminate (e.g. the full-cell design proposed in Ref. [1]) the electrode elongation will cause the battery cell to warp/twist during operation unless this mode of deformation is hindered. Moreover, uneven lithation of the fibres may cause the CF-SBE electrode to warp/twist. This can be seen from the variation in σ_{33} in the through thickness direction for the simulated case in Fig. 7e, where ε_{33} is assumed constant along the cross-section. Hence, to accurately predict and optimize the combined electro-chemo-mechanical response of battery cells utilizing CF-SBE electrodes, the electrode expansion needs to be carefully considered in the design in order to avoid damage/degradation and unwanted warping/deformation of the battery cell. Finally, it should also be noted that experimental studies by Jacques et al. [17] and Harnden et al. [18,19] have demonstrated a noticeable coupling effect between the open circuit voltage (OCV) and the applied strain in carbon fibres and CF-SBE electrodes. In Ref. [19], this coupling effect was utilized to make a strain-sensing, energy harvesting, structural carbon fibre composite material. In Ref. [39], we have shown that this coupling effect can be predicted by the utilized computational framework. Hence, the developed framework provides a tool for predicting the coupled electro-chemo-mechanical performance of CF-SBE electrode laminae under different loading conditions and for different applications.

4. Conclusions

In this paper, electrode laminae consisting of carbon fibres embedded in structural battery electrolyte (CF-SBE electrodes) are characterized utilizing experimental and numerical techniques. We perform experimental and numerical studies on CF-SBE electrode half-cells, and the results clearly show that the electrode thickness, transport properties of the SBE and applied current significantly affect the electrochemical performance. For example, the relative reduction in the specific capacities for the CF-SBE electrode, in comparison with an equivalent (i.e. same mass of carbon fibres) half-cell utilizing liquid

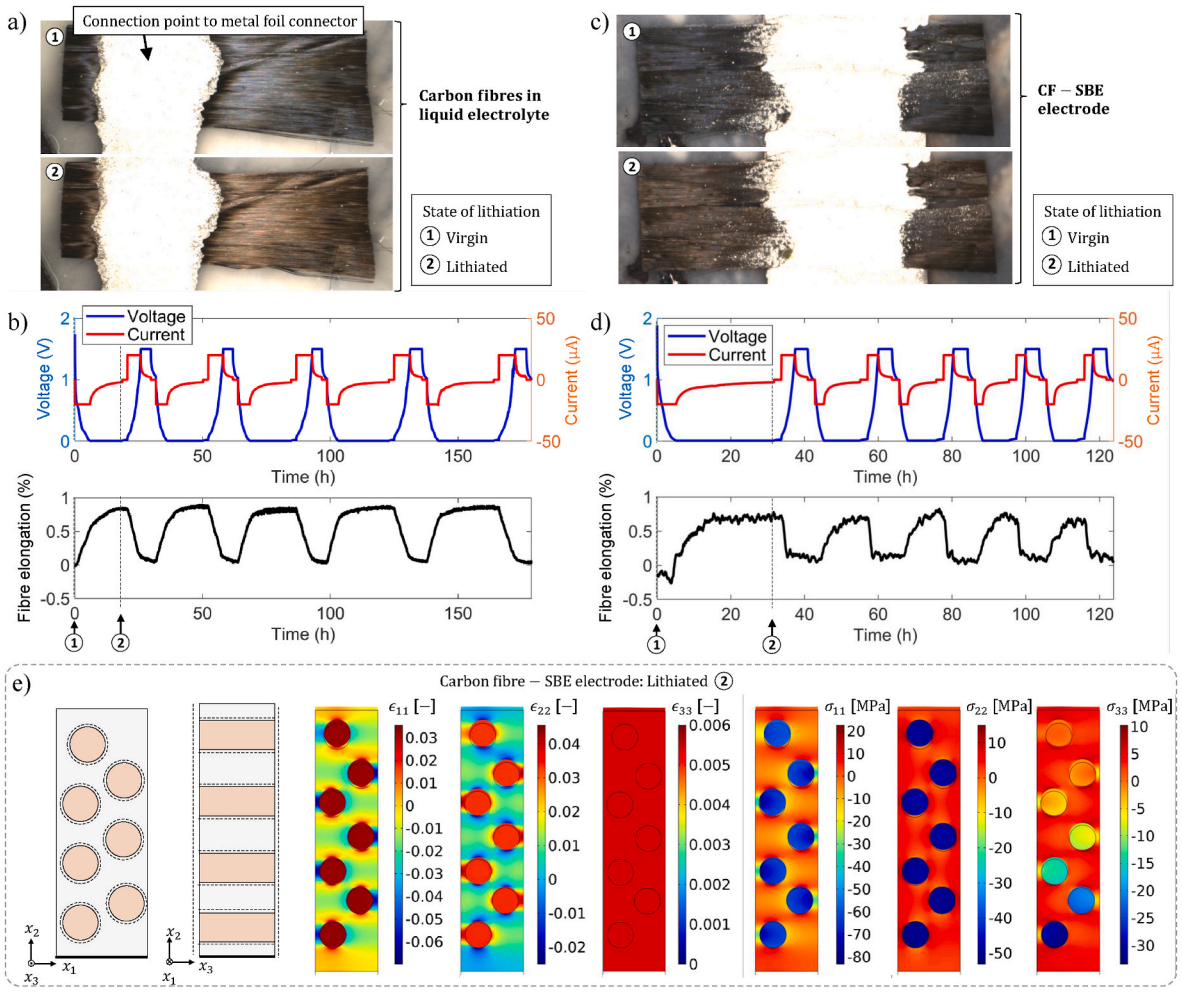

Fig. 7. (a) Photos of carbon fibre electrode in liquid electrolyte (reference sample, i.e. LE Sample) in virgin (1) and lithiated (2) state during DIC measurements. (b) Voltage, current and measured ("free") elongation of the carbon fibres in liquid electrolyte during the first 5 charge/discharge cycles. (c) Photos of CF-SBE electrode (SBE Sample) in virgin (1) and lithiated (2) state during DIC measurements. (d) Voltage, current and measured elongation of the CF-SBE electrode during the first 5 charge/discharge cycles. (e) Numerical estimates of mechanical strain (ϵ_{ii}) and stress components (σ_{ii}) in the CF-SBE electrode in the lithiated state (2), using Model 3.

electrolyte, are approximately 25% and 54% at applied currents 30 and 120 mA g^{-1} of carbon fibres, respectively. Moreover, increasing the electrode thickness of the studied CF-SBE electrode from 50 μm to 200 μm results in a reduction in specific capacity of approximately 70/95% for an applied current of 30/120 mA g^{-1} of fibres, respectively. Hence, the electrochemical performance is highly affected by the SBE and significant improvement in performance can be achieved by utilizing thin electrodes or by improving the transport properties of the SBE. It should be noted that the electrical losses associated with the impaired performance will generate heat. Since both the electrochemical and mechanical performance are highly influenced by the temperature [41], this is an important consideration to bear in mind in future work.

Further, we measure the Li-insertion induced longitudinal expansion of carbon fibre electrodes in liquid electrolyte and in CF-SBE electrodes during electrochemical cycling. In liquid electrolyte the total/reversible longitudinal expansions are found to be approximately 0.85/0.8%, respectively, while for the CF-SBE electrode lamina the reversible longitudinal expansion is found to be 0.6%. This fibre expansion gives rise to residual strains (and stresses) within the lamina, which is demonstrated numerically.

We demonstrate the capabilities of a previously developed computational framework [39] and compare numerical predictions with experimental data. Here, the theory is extended to account for the separator phase and its effective properties. Moreover, the model geometry, material data, etc., are based on experimental data. With respect to the electrochemical analysis, we demonstrate that the framework is able to capture the overall behaviour of the cell. However, due to model simplifications, linked to e.g. interface conditions, material properties, etc., the relaxation behaviour of the electric potential is not captured. Hence, further model refinements are needed to be able to capture the relaxation behaviour of the measured electric potential and to allow for using the modelling framework for optimization studies. This is planned to be the scope of future work.

With respect to the mechanical response, we show that the provided framework is able to predict strain and stress levels associated with insertion induced expansion/shrinkage of the fibres within the regime of small deformations and linear elastic material response. Further, due to the assumed stress/strain condition in the x_3 – direction, i.e. along the fibres, the three-dimensional stress state is captured even though the FE-analysis is two-dimensional while accounting for the highly anisotropic (transverse isotropic) character of the carbon fibres. It should be noted that in addition to the volume change, the properties of carbon fibres (e.g. the elastic moduli [58] and mobility coefficients [27]) are known to change with the degree of lithiation. Evaluation of the influence of such material characteristics on the electro-chemo-mechanical response will be the scope of future work. Further, to evaluate the strength of the material, the (multi-axial) stress state should be compared with limiting values (e.g. reported in Ref. [5]). However, to accurately evaluate the

strength of the studied material, more data is needed. For example, to measure the strength comprehensive sample preparation is required as e.g. discussed in Ref. [1] (in particular for certain failure modes). Moreover, to accurately predict the strength using the developed framework, suitable constitutive relations accounting for the coupled processes (and possibly also large strain kinematics) are needed.

Finally, the elastic modulus of the CF-SBE electrode in the fibre direction is in the order of 60 GPa. Remarkably, this is in the same range as several conventional construction materials e.g. aluminium.

Data availability

The data that support the findings of this study are available from the corresponding author upon request.

Authorship contributions

David Carlstedt: Conceptualization, Methodology, Software, Validation, Formal Analysis, Investigation, Data Curation, Writing - original draft, Visualization, Project administration.

Florian Rittweger: Methodology, Formal Analysis, Investigation, Data Curation, Visualization, Writing - review & editing.

Kenneth Runesson: Conceptualization, Methodology, Supervision, Funding acquisition, Writing - review & editing.

Adriana M. Navarro-Suárez: Formal Analysis, Investigation, Data Curation, Writing - review & editing.

Johanna Xu: Investigation, Writing - review & editing.

Shanghong Duan: Investigation, Writing - review & editing.

Fredrik Larsson: Methodology, Writing - review & editing.

Karl-Ragmar Riemschneider: Supervision, Funding acquisition, Writing - review & editing.

Leif E. Asp: Conceptualization, Methodology, Supervision, Funding acquisition, Writing - review & editing.

Declaration of competing interest

The authors declare that they have no known competing financial interests or personal relationships that could have appeared to influence the work reported in this paper.

Acknowledgements

This project has been funded by the European Union, Clean Sky Joint Undertaking 2, Horizon 2020 under Grant Agreement Number 738 085, USAF contract FA8655-21-1-7038, the Swedish National Space Agency, contract 2020-00 256, and the Swedish Research Council (VR) Grant no. 2020-05 057, which are gratefully acknowledged. The simulations were performed on resources at Chalmers Centre for Computational Science and Engineering (C3SE) provided by the Swedish National Infrastructure for Computing (SNIC). F.R. and K.R.R. acknowledges the financial support from the German Ministry for Economic Affairs and Energy (BMWi) within the project 'IMBAT' (grant ZF4019009RE7). A.M.N.S. acknowledges the financial support from Chalmers Battery Initiative, part of the profile Materials for Energy Applications jointly managed by the Areas of Advance Materials Science and Energy at Chalmers University of Technology.

Appendix A. Supplementary data

Supplementary data to this article can be found online at https://doi.org/10.1016/j.compscitech.2022.109283.

References

[1] L.E. Asp, et al., A structural battery and its multifunctional performance, Adv. Energy Sustain. Res. 2 (2021) 2000093, https://doi.org/10.1002/aesr.202000093.
[2] L.E. Asp, et al., Structural battery composites: a review, Funct. Compos. Struct. 1 (2019) 42001, https://doi.org/10.1088/2631-6331/ab5571.
[3] W. Fu, et al., Materials and technologies for multifunctional, flexible or integrated supercapacitors and batteries, Mater. Today (2021), https://doi.org/10.1016/j.mattod.2021.01.026.
[4] K. Moyer, et al., Carbon fiber reinforced structural lithium-ion battery composite: multifunctional power integration for CubeSats, Energy Storage Mater. 24 (2020) 676–681, https://doi.org/10.1016/j.ensm.2019.08.003.
[5] W. Johannisson, et al., Multifunctional performance of a carbon fiber UD lamina electrode for structural batteries, Compos. Sci. Technol. 168 (2018) 81–87, https://doi.org/10.1016/j.compscitech.2018.08.044.
[6] D. Carlstedt, L.E. Asp, Performance analysis framework for structural battery composites in electric vehicles, Composites Part B 186 (2020) 107822, https://doi.org/10.1016/j.compositesb.2020.107822.
[7] Y. Zhao, et al., Preparation and multifunctional performance of carbon fiber-reinforced plastic composites for laminated structural batteries, Polym. Compos. 41 (2020) 3023–3033, https://doi.org/10.1002/pc.25594.
[8] S. Yin, et al., Fabrication and multiphysics modeling of modified carbon fiber as structural anodes for lithium-ion batteries", J. Power Sources 476 (2020) 228532, https://doi.org/10.1016/j.jpowsour.2020.228532.
[9] M. Wang, et al., Biomimetic solid-state Zn2+ electrolyte for corrugated structural batteries, ACS Nano 13 (2019) 1107–1115, https://doi.org/10.1021/acsnano.8b05068.
[10] J.L. Lutkenhaus, P. Flouda, Structural batteries take a load off, Sci. Robot. 5 (2020), https://doi.org/10.1126/scirobotics.abd7026.
[11] S. Kalnaus, et al., Multifunctional approaches for safe structural batteries, J. Energy Storage 40 (2021) 102747, https://doi.org/10.1016/j.est.2021.102747.
[12] A.K. Kercher, J.O. Kiggans, N.J. Dudney, Carbon fiber paper cathodes for lithium ion batteries, J. Electrochem. Soc. 157 (2010) A1323, https://doi.org/10.1149/1.3495711.
[13] S.K. Martha, et al., Advanced lithium battery cathodes using dispersed carbon fibers as the current collector, J. Electrochem. Soc. 158 (2011) A1060, https://doi.org/10.1149/1.3611436.
[14] S. Ghosh, et al., Multifunctional utilization of pitch-coated carbon fibers in lithium-based rechargeable batteries, Adv. Energy Mater. 11 (2021) 2100135, https://doi.org/10.1002/aenm.202100135.
[15] T. Jin, et al., Bioinspired, tree-root-like interfacial designs for structural batteries with enhanced mechanical properties, Adv. Energy Mater. 11 (2021) 2100997, https://doi.org/10.1002/aenm.202100997.
[16] W. Johannisson, et al., Shape-morphing carbon fiber composite using electrochemical actuation, Proc. Natl. Acad. Sci. Unit. States Am. 117 (2020) 7658–7664, https://doi.org/10.1073/pnas.1921132117.
[17] E. Jacques, et al., Piezo-electrochemical effect in lithium-intercalated carbon fibres, Electrochem. Commun. 35 (2013) 65–67, https://doi.org/10.1016/j.elecom.2013.07.040.
[18] R. Harnden, D. Zenkert, G. Lindbergh, Potassium-insertion in polyacrylonitrile-based carbon fibres for multifunctional energy storage, morphing, and strain-sensing, Carbon 171 (2021) 671–680, https://doi.org/10.1016/j.carbon.2020.09.042.
[19] R. Harnden. Lightweight multifunctional composites: An investigation into ion-inserted carbon fibres for structural energy storage, shape-morphing, energy harvesting & strain-sensing (Doctoral Thesis), KTH Royal Institute of Technology, Stockholm, Sweden, 2021.
[20] W. Johannisson, D. Zenkert, G. Lindbergh, Model of a structural battery and its potential for system level mass savings, Multifunct. Mater. 2 (2019) 35002, https://doi.org/10.1088/2399-7532/ab3bdd.
[21] N. Ihrner, et al., Structural lithium ion battery electrolytes: via reaction induced phase-separation, J. Mater. Chem. 5 (2017) 25652–25659, https://doi.org/10.1039/C7TA04684G.
[22] L.M. Schneider, et al., Bicontinuous electrolytes via thermally initiated polymerization for structural lithium ion batteries, ACS Appl. Energy Mater. 2 (2019) 4362–4369, https://doi.org/10.1021/acsaem.9b00563.
[23] V. Tu, et al., Performance of bicontinuous structural electrolytes, Multifunct. Mater. 3 (2020) 25001, https://doi.org/10.1088/2399-7532/ab8d9b.
[24] M.H. Kjell, et al., PAN-based carbon fiber negative electrodes for structural lithium-ion batteries, J. Electrochem. Soc. 158 (2011) A1455–A1460, https://doi.org/10.1149/2.053112jes.
[25] W. Johannisson, et al., A screen-printing method for manufacturing of current collectors for structural batteries, Multifunct. Mater. 4 (2021) 35002, https://doi.org/10.1088/2399-7532/ac2046.
[26] G. Fredi, et al., Graphitic microstructure and performance of carbon fibre Li-ion structural battery electrodes, Multifunct. Mater. 1 (2018) 15003, https://doi.org/10.1088/2399-7532/aab707/meta.
[27] M.H. Kjell, et al., Electrochemical characterization of lithium intercalation processes of PAN-based carbon fibers in a microelectrode system, J. Electrochem. Soc. 160 (2013) A1473–A1481, https://doi.org/10.1149/2.054309jes.
[28] H. Zheng, et al., A comprehensive understanding of electrode thickness effects on the electrochemical performances of Li-ion battery cathodes, Electrochim. Acta 71 (2012) 258–265, https://doi.org/10.1016/j.electacta.2012.03.161.
[29] M. Singh, J. Kaiser, H. Hahn, Thick electrodes for high energy lithium ion batteries, J. Electrochem. Soc. 162 (2015) A1196–A1201, https://doi.org/10.1149/2.0401507jes.
[30] T. Danner, et al., Thick electrodes for Li-ion batteries: a model based analysis, J. Power Sources 334 (2016) 191–201, https://doi.org/10.1016/j.jpowsour.2016.09.143.

[31] X. Lu, et al., 3D microstructure design of lithium-ion battery electrodes assisted by X-ray nano-computed tomography and modelling, Nat. Commun. 11 (2020) 2079, https://doi.org/10.1038/s41467-020-15811-x.
[32] H. Sun, et al., Hierarchical 3D electrodes for electrochemical energy storage, Nat. Rev. Mater. 4 (2019) 45–60, https://doi.org/10.1038/s41578-018-0069-9.
[33] R. Tian, et al., Quantifying the factors limiting rate performance in battery electrodes, Nat. Commun. 10 (2019) 1933, https://doi.org/10.1038/s41467-019-09792-9.
[34] S.E. Trask, et al., From coin cells to 400 mAh pouch cells: enhancing performance of high-capacity lithium-ion cells via modifications in electrode constitution and fabrication, J. Power Sources 259 (2014) 233–244, https://doi.org/10.1016/j.jpowsour.2014.02.077.
[35] M. Ebner, et al., Tortuosity anisotropy in lithium-ion battery electrodes, Adv. Energy Mater. 4 (2014) 1301278, https://doi.org/10.1002/aenm.201301278.
[36] Y. Dai, V. Srinivasan, "On graded electrode porosity as a design tool for improving the energy density of batteries", J. Electrochem. Soc. 163 (2016) A406–A416, https://doi.org/10.1149/2.0301603jes.
[37] K. Xu, Nonaqueous liquid electrolytes for lithium-based rechargeable batteries, Chem. Rev. (2004) 4303–4417, https://doi.org/10.1021/cr030203g.
[38] E. Jacques, et al., Expansion of carbon fibres induced by lithium intercalation for structural electrode applications, Carbon 59 (2013) 246–254, https://doi.org/10.1016/j.carbon.2013.03.015.
[39] D. Carlstedt, et al., Electro-chemo-mechanically coupled computational modelling of structural batteries, Multifunct. Mater. 3 (2020) 45002, https://doi.org/10.1088/2399-7532/abc60d.
[40] D. Carlstedt, E. Marklund, L.E. Asp, Effects of state of charge on elastic properties of 3D structural battery composites, Compos. Sci. Technol. 169 (2019) 26–33, https://doi.org/10.1016/j.compscitech.2018.10.033.
[41] D. Carlstedt, L.E. Asp, Thermal and diffusion induced stresses in a structural battery under galvanostatic cycling, Compos. Sci. Technol. 179 (2019) 69–78, https://doi.org/10.1016/j.compscitech.2019.04.024.
[42] J. Xu, G. Lindbergh, J. Varna, Carbon fiber composites with battery function: stresses and dimensional changes due to Li-ion diffusion, J. Compos. Mater. 52 (2018) 2729–2742, https://doi.org/10.1177/0021998317752825.
[43] J. Xu, G. Lindbergh, J. Varna, Multiphysics modeling of mechanical and electrochemical phenomena in structural composites for energy storage: single carbon fiber micro-battery, J. Reinforc. Plast. Compos. 37 (2018) 701–715, https://doi.org/10.1177/0731684418760207.
[44] F. Dionisi, R. Harnden, D. Zenkert, A model to analyse deformations and stresses in structural batteries due to electrode expansions, Compos. Struct. 179 (2017) 580–589, https://doi.org/10.1016/j.compstruct.2017.07.029.
[45] J. Newman, W. Tiedemann, Porous electrode theory with battery applications, AIChE J. 21 (1975) 25–41, https://doi.org/10.1002/aic.690210103.
[46] M. Doyle, T.F. Fuller, J. Newman, Modeling of galvanostatic charge and discharge of the lithium/polymer/insertion cell, J. Electrochem. Soc. 140 (1993) 1526, https://doi.org/10.1149/1.2221597.
[47] M. Doyle, J. Newman, The use of mathematical modeling in the design of lithium/polymer battery systems, Electrochim. Acta 40 (1995) 2191–2196, https://doi.org/10.1016/0013-4686(95)00162-8.
[48] J. Newman, K.E. Thomas-Alyea, Electrochemical Systems. The ECS Series of Texts and Monographs, Wiley, 2004.
[49] F. Rittweger, et al., Investigation of charge carrier dynamics in positive lithium-ion battery electrodes via optical in situ observation, J. Power Sources 482 (2021) 228943, https://doi.org/10.1016/j.jpowsour.2020.228943.
[50] V. Roscher, F. Rittweger, K.-R. Riemschneider, Electrochromic effect of indium tin oxide in lithium iron phosphate battery cathodes for state-of-charge determination, ACS Appl. Mater. Interfaces 11 (2019) 6900–6906, https://doi.org/10.1021/acsami.8b16439.
[51] M.Z. Bazant, III. Lecture 10: Li-ion batteries. Lecture notes in 10.626 Electrochemical energy systems. MIT Open Course Ware. https://ocw.mit.edu/courses/chemical-engineering/10-626-electrochemical-energy-systems-spring-2014/lecture-notes/MIT10_626S14_S11lec10.pdf, 2014.
[52] M.Z. Bazant, II. Equilibrium thermodynamics lecture 8: the Nernst equation. Lecture notes in 10.626 Electrochemical energy systems. MIT Open Course Ware. https://ocw.mit.edu/courses/chemical-engineering/10-626-electrochemical-energy-systems-spring-2014/lecture-notes/MIT10_626S14_S11lec08.pdf, 2014.
[53] R. Xu, et al., Heterogeneous damage in Li-ion batteries: experimental analysis and theoretical modeling, J. Mech. Phys. Solid. 129 (2019) 160–183, https://doi.org/10.1016/j.jmps.2019.05.003.
[54] S.E. Okan, D.C. Champeney, Molar conductance of aqueous solutions of sodium, potassium, and nickel trifluoromethanesulfonate at 25‡C, J. Solut. Chem. 26 (1997) 405–414, https://doi.org/10.1007/BF02767679.
[55] S. Indris, et al., Ionic liquid based electrolytes: correlating Li diffusion coefficients and battery performance, J. Electrochem. Soc. 161 (2014) 2036–2041, https://doi.org/10.1149/2.0131414jes.
[56] J.F. Snyder, E.L. Wong, C.W. Hubbard, Evaluation of commercially available carbon fibers, fabrics, and papers for potential use in multifunctional energy storage applications, J. Electrochem. Soc. 156 (2009) A215–A223, https://doi.org/10.1149/1.3065070.
[57] C. Lee, et al., Optimized microstructures for multifunctional structural electrolytes, Multifunct. Mater. 2 (2019) 45001, https://doi.org/10.1088/2399-7532/ab47ed.
[58] S. Duan, et al., Effect of lithiation on the elastic moduli of carbon fibres, Carbon 185 (2021) 234–241, https://doi.org/10.1016/j.carbon.2021.09.037.
[59] G. Taillades, J. Sarradin, Silver: high performance anode for thin film lithium ion batteries, J. Power Sources 125 (2004) 199–205, https://doi.org/10.1016/j.jpowsour.2003.07.004.
[60] A. Shellikeri, et al., Investigation of pre-lithiation in graphite and hard-carbon anodes using different lithium source structures, J. Electrochem. Soc. 164 (2017) A3914–A3924, https://doi.org/10.1149/2.1511714jes.
[61] R.A. Schapery, Thermal expansion coefficients of composite materials based on energy principles, J. Compos. Mater. 2 (1968) 380–404, https://doi.org/10.1177/002199836800200308.
[62] J. Xu, et al., Characterization of the adhesive properties between structural battery electrolytes and carbon fibers, Compos. Sci. Technol. 188 (2020) 107962, https://doi.org/10.1016/j.compscitech.2019.107962.